Data Repository Item

APPENDIX

Sites

Beiguoyuan (36° 37' 36.2"N, 107° 16' 57.4"E, 1545 m a.s.l) is located near Huanxian, Gansu Province on the northwestern Loess Plateau. Sampling concentrated on the upper 12.6 m, including the Black Loam and upper Malan Loess formations. At Xunyi, Shaanxi Province (35° 01' 25.1"N, 108° 12' 21.2"E, 1151 m a.s.l) on the central Loess Plateau, strata were sampled over the upper 6.65 m to include the entire Black Loam and upper Malan Loess. Sampling for grain-size and magnetic susceptibility was conducted at 5 cm intervals, while samples for optically stimulated luminescence (OSL) dating were taken at 10-40 cm at Beiguoyuan and 20 cm at Xunyi (Figure DR1). Xunyi experiences considerably more annual rainfall than Beiguoyuan at present (~600 mm compared to ~500 mm) and is further away from hypothesized sediment sources (Figure 1 in accompanying paper). As this affects the sedimentary and diagenetic context of the study sites, and consequently the sedimentary- and pedo-facies, it is important to keep this in mind when interpreting OSL and climate proxy data. It should also be noted that a detailed record of climate proxy changes is preserved down to L2 at the sections, approximately marine oxygen-isotope stage (MIS) 6 in age (Figure DR2). Thus, the general sedimentary stratigraphy of the sites is typical for loess tableland (yuan) sequences (e.g. Nugteren and Vandenberghe, 2004).

Sampling

Samples for OSL dating were collected as 10x10x10 cm blocks or in metal tubes hammered into the cleared and cleaned section face. Samples were wrapped in light-tight black plastic bags immediately after being removed from the sections and were processed in the Oxford University Luminescence Dating Laboratory under subdued red light. Sunlight-exposed outer surfaces of blocks and the ends of tube samples were excluded from equivalent dose (D_e) determinations but retained for radioisotope measurements (to determine dose rate). Carbonates and organic matter were removed from the D_e (unexposed) fractions using 0.1 M HCl and 15% H_2O_2. Quartz was isolated by immersion in 35% H_2SiF_6 for between 2 and 4 weeks with a subsequent 0.1 M HCl wash to remove fluorite precipitates (Berger et al., 1980). The coarse silt fraction (40-63 μm) was obtained by wet sieving.

SAR Procedure

More complete details of the analytical techniques and internal tests used in age determination are presented elsewhere (Stevens et al., 2007a). D_e values were measured using the SAR procedure (Murray and Wintle, 2000) or using a standardized growth curve (Roberts and Duller, 2004) (see below) performed on a Risø TL-DA-15 TL/OSL reader (Figure DR3). A blue LED (λ = 470±20 nm) stimulation source was used (60 s, c. 400 mJ cm^{-1}) on samples and the OSL signal was measured using a 9235QA photomultiplier tube filtered by 6 mm of Hoya U340 (Bøtter-Jensen et al., 2000). The signal was integrated from the first 0.6 s of stimulation minus a background estimated from the last 6 s of stimulation. All growth curves were fitted using a saturating exponential plus linear function. Aliquots yielding recycling ratios (Murray and Wintle, 2000) or IR depletion ratios (Duller, 2003) differing from unity by greater than 10% were rejected. The uncertainty on individual D_e

values was estimated using Monte Carlo simulation and a weighted mean D_e (with one standard error uncertainty) was calculated for each sample (typically ~14 aliquots).

Standardized Growth Curves

In order to increase the efficiency of obtaining ages, the equivalent doses of certain samples were obtained through construction of standardized growth curves (SGC). Roberts and Duller (2004) suggest that when using the SAR technique, which normalizes all data to the luminescence intensity observed using a fixed "test dose", quartz may exhibit a uniform response to laboratory dose and thus growth curves for samples from the same site or region will be identical within errors. Roberts and Duller (2004) utilized this principle to construct SGCs for different sediments. An SGC is constructed through calculation of mean sensitivity-corrected luminescence intensity (L_x/T_x) multiplied by the test dose (TD) in Gy [$(L_x/T_x)TD$] for each dose point in the growth curve. Equivalent doses can therefore be calculated for aliquots where only the sensitivity-corrected natural luminescence intensity has been measured. This approach can facilitate high-resolution dating of Chinese loess by dramatically increasing sample throughput (Stevens et al., 2007a).

Two SGCs were constructed for the strata above and below 5.4 m depth at the Beiguoyuan section, along with a single curve for Xunyi samples (Figure DR4). For each SGC, 9-10 samples (generally comprising a minimum of 100 aliquots) were used to constrain five regeneration dose points (Table DR1) that fully encompass the likely natural range of equivalent doses for relevant samples. A standard saturating exponential + linear [$I = I_o + I_{max} (1-e^{-D/Do}) + D.g$ (Roberts and Duller, 2004)] function was then applied to define the curve and Monte Carlo simulation used to calculate D_e and errors based on a natural,

test dose corrected signal. The validity of this approach was tested for each SGC by comparing equivalent doses calculated using the relevant curve with those derived from a standard SAR measurement (not used to construct the SGC). Figure DR5 shows equivalent doses with errors calculated using the SGCs in Figure DR4, plotted against those obtained using standard SAR D_e values. Equivalent doses calculated using SGCs are almost all identical within errors to those obtained through the standard SAR technique, confirming the applicability of an SGC approach in this case. Thus, equivalent doses were calculated for many of the samples from the Beiguoyuan and Xunyi sections using the SGC measured for that site and depth (Tables DR1 and DR2). Equivalent doses obtained using an SGC seem to fit stratigraphically with the remaining equivalent doses calculated using standard SAR (Table DR2), reinforcing the accuracy of the approach.

The rationale for the choice of 5.4 m depth for construction of a lower Beiguoyuan SGC was based on the need to better constrain samples exhibiting equivalent doses closer to 100 Gy. In addition, despite Lai (2006) suggesting that a universal growth curve was applicable to Chinese loess deposits, other investigations suggest it is more prudent to apply an individual curve for each section studied (Stevens et al., 2007a). Indeed application of t-tests to L_x/T_x values of overlapping regeneration points for each SGC indicate that these sets cannot be considered from the same population at >99% certainty (Table DR3). Thus, the more conservative approach of Roberts and Duller (2004) and Burbidge et al. (2006) is followed, whereby a unique SGC is constructed for each section (or parts of sections) studied using 4-6 regeneration points, as would occur in a standard SAR analysis (Murray and Wintle, 2000). Whilst it may be desirable to better constrain the SGC through the use of more regeneration points (as it would with a standard SAR sequence), it is here viewed

as inappropriate to combine L_x/T_x data from multiple sites or sections in the compilation of a 'universal' growth curve or an SGC that is applicable to a large sedimentary depocenter such as the Loess Plateau (e.g. Lai, 2006). More research is required to determine how to define the stratigraphic limits for SGCs from a particular site.

Dose Rates

Dose rates were calculated from uranium, thorium and potassium contents measured using Inductively Coupled Plasma Mass Spectrometry (ICP-MS) and Atomic Emission Spectrometry (-AES). ICP samples were prepared by lithium metaborate or sodium peroxide fusion. Dose rates were calculated with a water content of 8±4% based on current moisture contents determined in the laboratory (see below), and an alpha efficiency of 0.04±0.02 (Rees-Jones, 1995). Alpha and beta attenuation was obtained using calculations in Bell (1980) and Mejdahl (1979) respectively and dose rate conversion factors were taken from Adamiec and Aitken (1998). Uncertainties are based on the propagation, in quadrature, of individual errors for all measured quantities, which if unknown are taken as 10%. In addition to uncertainties calculated from counting statistics, errors due to 1) beta source calibration (3%) (Armitage and Bailey, 2005), 2) radioisotope concentration (3%), 3) dose rate conversion factors (3%) and 4) attenuation factors (3%) have been included (Murray and Olley, 2002). The cosmic dose was calculated using present day burial depth (Prescott and Hutton, 1994). D_e, dosimetry and age data are presented in Table DR2.

The estimation of current and past water contents forms a considerable limitation to the accuracy of luminescence dating (e.g. Aitken, 1998). Full details of the procedure used in this study are presented in Stevens et al. (2007a). Water contents (as a proportion of wet

weight) obtained from individual samples analyzed (upper 30 samples) from the study sites (Figure DR6) show values considerably lower than expected from previous studies (e.g. Lai and Wintle, 2006). In addition, while values seem to show a drop from ~2.7-1.8% at Beiguoyuan from S0 to L1 strata, there is very little trend in the data. When water content values were obtained from air tight pots taken at less frequent portable γ-spectrometry measurement intervals (Stevens et al., 2007a), significantly higher values are obtained (Table DR4), more in line with expected values. However, such data do not allow the use of sample specific water contents in dose rate calculation.

In any case, it is suggested that the use of individual water contents obtained for each sample may be misleading. Variables such as recent weather, section aspect, drainage direction and exposure history of the section will likely limit the use of sample specific water contents as a first order approximation of the relative differences in water content since deposition. For this reason, and due to the likely incorrect sample specific water contents, a mean water content of 8±4%, derived from data in Table DR4 was used in this study for both sections. The errors on this value encompass most of the range of variability at the sample sites and while Table DR4 shows that water contents are higher at Xunyi, this seems just as likely due to significant precipitation events occurring just prior to sampling of this site, rather than a long-term difference. Thus, the mean value not only represents the mean of water contents from the study sites (as well as values from Xifeng and Shiguanzhai (Stevens et al., 2006)), it can be considered to combine a recently wetted section with one that had not experienced such conditions at the time of sampling. As such, the mean value presented here may better represent the range of variability in water content since deposition, rather than suggest a more precise (but likely misleading) sample specific value.

It should also be stated that while some paleosol samples exhibited higher water contents (Table DR4), this was not always the case and will again have been complicated by the precipitation events before and during sample collection.

In order to determine how valid the application of a standard water content was in this study, ages were calculated for sample CH04/1/1 (Beiguoyuan) based on the standard water content (7.91±0.44 ka) and extreme values set at 13±10% (8.32±0.58 ka) and 2.5±10% (7.46±0.55 ka). These ages demonstrate that even when these water content values (at the extreme ends of measured variability) are taken, the change in age is within the 1σ error range of the age calculated using 8±4% (i.e. <5.5%). Thus, the findings of this study that are based on the OSL ages cannot be attributed to variability in water content of samples.

Age Model Derivation

The use of high frequency and systematic sampling enables the construction of age-depth relationships for strata at the sites. As the OSL results demonstrate the existence of individual strata with relatively consistent age increase with depth (and therefore sedimentation rate), an age model can be constructed by taking the maximum and minimum OSL ages of samples in such strata of identical sedimentation rate, and linearly interpolating ages between. This technique was applied to both study sites and strata were identified based on visual identification of changes in age increase with depth (Figure DR7). Calculation of errors for this age model using standard propagation of OSL errors in quadrature leads to values of less than 3% and does not accurately reflect the true error on individual OSL ages. In order to overcome this, an alternative method of error derivation

was used. Individual errors on the maximum and minimum ages were averaged for each individual stratum of unchanging sedimentation rate. This error, normally between 5 and 7%, and therefore more accurately reflecting individual OSL ages, was then applied to the interpolated ages over the whole stratum. For the Xunyi age model, ages for samples CH04/3/9, 15 and 22 have been calculated using the dose rate of the stratigraphically higher sample. This was necessary because calculated dose rates for these samples lie well beyond the 1σ bounds for all other samples at this site and are likely to be erroneous, potentially due to instrument error.

Excluded Samples

At Beiguoyuan, ages for samples between 3.1 and 5.4 m have been excluded from construction of the age model. These samples display anomalously high age and equivalent dose (OSL ages up to 15% older than expected from ages from surrounding units). Dose recovery tests were used on a high proportion of samples in this section, as well as on a smaller proportion of samples from elsewhere in the section. During a dose recovery test, 12-14 aliquots of a sample were bleached using a blue LED (90% power, $\lambda = 470 \pm 20$ nm) at room temperature for 200 s, followed by a 10,000 s pause and then 200 s of further stimulation. Following a further 60 s room temperature bleach, a laboratory administered β -dose approximately equal to the expected or previously obtained D_e was then given to the aliquots, followed by measurement using a standard SAR sequence (Figure DR3). The samples were deemed to have failed a dose recovery test when the ratio of recovered to given doses deviated from unity by >10%. The applied SAR/SGC protocol is unlikely to determine a correct age for samples which fail the dose recovery test. Results show that

183 many, but not all, of the samples between 3.1 and 5.4 m at Beiguoyuan show overestimates
184 of the given dose (Figure DR8). When these results are plotted by depth (Figure DR9)
185 many samples in the 3.1 to 5.4 m depth range exhibit ratios beyond 10% of unity, while no
186 samples lie outside this boundary in the remainder of the dataset. Acceptable dose recovery
187 ratios are obtained for given doses up to 160 Gy, indicating that the 70 Gy upper limit for
188 the successful application of SAR to loess (suggested by Stevens et al. 2007a) may not be
189 correct. However, dose recovery tests do indicate a systematic overestimate of the given
190 dose calculated at 6.1% using linear regression (Figure DR9b). While at present there is no
191 explanation for this, it is important to note that it will not affect the age model and
192 paleoclimatic findings of this study as the offset is smaller than the final D_e and age errors.

193 To further investigate the excluded samples, the average L_x/T_x (sensitivity corrected
194 luminescence intensity) values of the first 20 Gy dose point (20 Gy test dose) in the SAR
195 sequence was plotted by depth (Figure DR10). This shows that in general, the test dose
196 OSL response is similar to the initial dose response for many samples (i.e. the ratios are
197 close to unity). However, many of the samples between 3.1 and 5.4 m depth show a
198 reduced L_x/T_x value indicating a larger test dose response than regenerated OSL response to
199 a 20 Gy dose. As with the dose recovery experiments, not all samples in the affected strata
200 exhibit this tendency. Strangely, the samples that exhibit this tendency do not all exhibit
201 failed dose recoveries (Figure DR8) or show a larger than expected age (Figure DR7) and
202 vice versa. While the reason for this inconsistency is unclear, it should be noted that an
203 accurate dose recovery does not require the acceptance of an OSL age when other evidence
204 suggests ages may be inaccurate (Murray and Wintle, 2000). For this reason the entire
205 section where this combined evidence is apparent is excluded from age model calculation.

In addition, while it is noted that dose recovery overestimates can be of the order of a factor of 2 (Figures DR8 and DR9), contrasting with the apparent maximum 20% D_e overestimate for excluded samples shown in Table DR2, this does not affect the findings of the study as pertinent to the construction of the age model and the climatic interpretation. Samples that fail a dose recovery test need to be rejected irrespective of what is shown by the natural D_e obtained from these samples.

While a more thorough investigation of the reasons for this combined evidence is beyond the scope of this analysis, there are a number of possible explanations that can be hypothesized. Comparison of the natural and 20 Gy test dose decay curves indicate that there is no substantial difference in the shape between samples from above and below, versus within the excluded region (Figure DR11). There is however, slightly more variability in the samples with anomalously high ages and some of the variability seems to be expressed in terms of larger peak values. By calculating the ratios of recovered to given doses using different signal integration limits for samples surrounding and within the strata excluded from age model calculation, the effect of changing the part of the luminescence decay curve used for D_e determination can be examined. Figure DR12 shows the outcome of two such calculations, one for a sample within the anomalous unit at Beiguoyuan, and one from above. Figure DR12a shows ratios of recovered to given dose using different integration limits for sample CH04/1/80, taken from below the 5.4 m depth, while Figure DR12b shows the same but for sample CH04/1/33, taken from within the 3.1-5.4 m unit. The general characteristics of all samples from the surrounding strata are similar to that shown for CH04/1/80. Some samples within the strata with excluded ages also show similar characteristics to CH04/1/80, however many exhibit behavior similar to CH04/1/33.

CH04/1/33 shows a strong dependence of recovered dose on signal integration limits. Conversely, all integration limits used on CH04/1/80 yield ratios of recovered to given dose within 10% of unity. It seems that with many samples from the anomalous unit, only integration limits that reduce the influence of the initial decay component yield dose recovery ratios within 10% of unity. The integration limits used in this study do not therefore appear to yield realistic age estimates in many of these excluded samples. Further investigation is needed into the luminescence decay curve properties of the studied samples in order to clarify this situation.

Other potential explanations for the anomalous ages in the excluded samples include feldspar contamination and water content changes. As samples have all passed an IR test for feldspar contamination (Duller, 2003) and show no observable 220° C TL peaks, it seems unlikely that feldspar contamination would cause the changes in D_e. Some studies (e.g. Roberts and Wintle, 2001; Stokes et al., 2003) have used an IR bleach added on to the SAR sequence, prior to initial and test dose response stimulation. However, as such an IR bleach would affect only that OSL component measured by an IR test (Duller, 2003), there is no *a priori* reason to suggest that applying an IR bleach would remove any unstable feldspar OSL decay component not detected using an IR test (Duller, 2003). In addition, as demonstrated above, the recorded variability in ages created by possible water content changes (<5.5%) (Table DR4) cannot cause the significant changes in age (~15%) in this section. An increase in sand content is evident at this level (Figure DR2), although comparison of porosity values for the coarsest (CH04/1/41) and finest (CH04/3/3) grain-size samples in this study (0.5 and 0.53 respectively) show that this is unlikely to alter long-term water content. Conversely, the change in grain-size may suggest that different source

regions have become involved in loess sedimentation, bringing grains that cannot be dated using the standard procedure successfully applied to other grains at the sites, and certainly implies that a different depositional regime occurred over this interval. Finally, due to the fact that both SAR and SGC processed samples exhibit this anomalous behavior and because the dose recovery tests show problems with the SAR protocol applied, the source of this anomalous behavior cannot be attributed to the use of SGCs.

It therefore seems likely that the high sedimentation rate event, the luminescence behavior of the samples (Figures DR9; DR10 and DR12) and the high grain-size values at this point are all related, potentially to a source change, and require further investigation. However, for the purposes of this study, as these samples occur within a stratum exhibiting an extremely high sedimentation rate, they can be considered to be coeval with over and underlying sediments. It is important to note that considering these sediments as either eolian or non-eolian (and consequently including or excluding them in sedimentation rate calculation) has no significant effect on the age model or proxy reconstruction (Figure DR13). As such, while the sample ages are rejected (as failing internal tests), in the absence of stratigraphic or definitive grain-size evidence that suggests these sediments are not eolian, the proxy values are included within the reconstructions presented in the accompanying paper.

At Xunyi, samples between 145 and 255 cm have also been excluded from the age model. This exclusion is based on the hypothesis that the substantial variation in age with depth exhibited over this interval is due to enhanced bioturbation and re-exposure of previously deposited sediments during pedogenesis (Stevens et al., 2006). This hypothesis is based on a number of lines of evidence. Firstly, the observed variability occurs at the

base of the Holocene soil, precisely where increased bioturbation would be expected to occur. Indeed, Bateman et al. (2003) demonstrated that OSL ages can indeed be significantly altered by pedoturbation and where sampling is not systematic this may lead to errors in the interpretation of ages. Secondly, this same pattern of disturbance occurs at Xifeng and Shiguanzhai (also in the central and southern Loess Plateau) but not at Beiguoyuan (Stevens et al., 2006). Given the current depositional and climatic regime at the sites (Figure 1 in accompanying paper), this suggests that only the enhanced soil forming conditions in the center and south of the Loess Plateau are sufficient for bioturbation to take place. Indeed, the longest (in terms of age) affected record comes from Shiguanzhai, where soil forming conditions are strongest and sedimentation lowest (Stevens et al., 2006). Thirdly, there is no accompanying change in dose rate. The variability in age is generally only reflected in D_e, although the U value of CH04/3/9 is anomalously high (Table DR2). However, even for this sample changing the U value to average levels still leaves the sample ~3.5 ka younger than the overlying sample and ~9.5 ka younger than the underlying one. This D_e variability therefore suggests that changes in sediment composition, source region changes or radioactive disequilibrium are unlikely to account for the age inversions. While grain-size does increase in this part of the section, this is also unlikely to cause variability in water content large enough to affect age calculation (see above). Indeed, grain-size values are still considerably lower than at Beiguoyuan where the majority of ages increase consistently down section. Another explanation could involve non-eolian deposition. However, the bioturbation explanation is here favored largely due to the absence of evidence contrary to eolian sedimentation and the coincidence of these units with the bases of soils, likely to be more influenced by bioturbation. This evidence also

298 strongly suggests that partial bleaching is an unlikely explanation. Nonetheless, these
299 alternative hypotheses require testing using independent methods such as anisotropic
300 magnetic susceptibility, single grain OSL studies on coarser grains, or detailed soil
301 micromorphology (e.g. Kemp and Derbyshire, 1998).
302
303 **Proxies**
304 By applying the OSL based age models to the regularly spaced climate proxy measures,
305 climate reconstructions plotted on a continuous age axis can be developed that are free from
306 arbitrary links to insolation or marine oxygen-isotope stratigraphy (Figure DR14).
307 However, it is important to note that the averaging of OSL ages and interpolation of
308 individual ages in the manor necessary to derive a time-continuous age model as above,
309 will come at the expense of some smaller scale changes in age and sedimentation.
310 However, it is also important to note that this decreased precision, as compared to
311 individual ages, does not prevent the application of our age model to centennial-millennial
312 scale climate reconstructions, as in the accompanying paper.
313 As sedimentation rate data from OSL dating are relatively new in the literature, the
314 sedimentation rate calculation used here is described in the accompanying paper.
315 Sedimentation rates are presented in Table DR5. Samples for magnetic susceptibility
316 analysis were pre-treated by air drying, disaggregation and sieving at 2 mm prior to
317 weighing and measurement in 25 x 25 mm diamagnetic pots. Measurements were taken
318 using high (4.7 kHz) and low (0.47 kHz) frequency fields at high sensitivity (0.1) using a
319 Bartington MS2 magnetic susceptibility meter. Bulk low frequency susceptibility (χ_{lf}) and
320 high frequency susceptibility (χ_{hf}) measurements are given in units of m^3kg^{-1} and %

frequency dependence (χ_{fd}) is defined as (χ_{lf} - χ_{hf})/ χ_{lf}. Frequency dependence is intended to estimate the relative contribution of fine viscous grains at the border between superparamagnetic and single domain to the total ferromagnetic assemblage (Dearing et al., 1996). It has been suggested that magnetic susceptibility changes correspond to changes in summer monsoon induced weathering, with the single domain and total ferromagnetic assemblage the most sensitive indicator of the East Asian southeast monsoon (Maher and Thompson, 1991). However, χ_{lf} is used in this study as calculated errors associated with χ_{fd} make its use problematic (Table DR6). Grain-size measurements were made using a Cilas 920 laser granulometer after preparation according to the method outlined in Sun et al. (2002). Multiple grain-size statistics were calculated through the GRADISTAT program (Blott and Pye, 2001) using the Folk and Ward (1957) and moments methods. The reproducibility of grain-size and magnetic susceptibility methods are given in Table DR6, estimated by repeating machine measurements 20 times on two samples presented in Stevens et al. (2006; 2007b).

By isolating the coarse silt and sand fraction, the influence of higher altitude winds involved in the transport of fine silt and clay can be removed from the investigation (Lu et al., 1999). High altitude winds are associated with the westerly jet stream while lower altitude and surface winds over China are associated with the northwest monsoon circulation (Sun, 2004). The coarse silt and sand component will therefore likely better reflect the influence of monsoon circulation over the Loess Plateau and is shown to exhibit considerable variation in relation to other grain-size categories (Figure DR15). Thus the >30 μm fraction is utilized in this study. Nevertheless, the influence of sediment supply may have a significant affect on sedimentation rate, and potentially grain-size. Indeed,

sedimentation rate changes are probably the result of a complex interaction between the influence of winter monsoon controlled source aridity and wind speed as well as local site specific conditions and vegetation (Stevens et al., 2007b). While sediment supply does not appear to be the main limiting factor on sedimentation during the Quaternary (Sun, 2002), and based on modeling is also unlikely to be at present (Zhang et al., 2003), it is wise to use caution when interpreting grain-size, and particularly sedimentation rates, in terms of the winter monsoon.

REFERENCES CITED

Adamiec, G., and Aitken M.J., 1998, Dose rate conversion factors: update: Ancient TL, v. 16, p. 37-50.

Aitken, M.J., 1998, An introduction to optical dating: Oxford University Press, UK, p. 267.

Armitage, S.J., and Bailey R.M., 2005, The measured dependence of laboratory beta dose rates on sample grain size: Radiation Measurements, v. 39, p. 123-127.

Bateman, M.D., Frederick, C.D., Jaiswal M.K., and Singhvi, A.K., 2003, Investigations into the potential effects of pedoturbation on luminescence dating: Quaternary Science Reviews, v. 22, p. 1169-1176.

Bell, W.T., 1980, Alpha dose attenuation in quartz grains for thermoluminescence dating: Ancient TL, v. 12, p. 4-8.

Berger, G.W., Mulhern, P.J., and Huntley, P.J., 1980, Isolation of silt-sized quartz from sediments: Ancient TL, v. 11, p. 8-9.

365 Blott, S.J., and Pye K., 2001, GRADISTAT: A grain size distribution and statistics package
366 for the analysis of unconsolidated sediments: Earth Surface Processes and Landforms, v.
367 26, p. 1237-1248.
368 Bøtter-Jensen, L., Bulur, E., Duller, G.A.T., and Murray, A.S., 2000, Advances in
369 luminescence instrumentation: Radiation Measurements, v. 32, p. 523-528.
370 Burbidge, C.I., Duller, G.A.T., and Roberts, H.M., 2006, D_e determination for young
371 samples using the standardised OSL response of coarse-grain quartz: Radiation
372 Measurements, v. 41, p. 278-288.
373 Dearing, J., Dann, R.J.L., Hay, K., Lees, J.A., Loveland, P.J., Maher, B.A., and O'Grady
374 K., 1996, Frequency-dependent susceptibility measurements of environmental materials:
375 Geophysics Journal International, v. 124, p. 228-240.
376 Duller, G.A.T., 2003, Distinguishing quartz and feldspar in single grain luminescence
377 measurements: Radiation Measurements, v. 37, p. 161-165.
378 Folk, R.L., and Ward W.C., 1957, Brazos River bar: a study in the significance of grain size
379 parameters: Journal of Sedimentary Petrology, v. 27, p. 3-26.
380 Kemp, R.A., and Derbyshire, E., 1998, The loess soils of China as records of climatic
381 change: European Journal of Soil Science, v. 49, p. 525-539.
382 Lai, Z.P., 2006, Testing the use of an OSL standardised growth curve (SGC) for D_e
383 determination on quartz from the Chinese Loess Plateau: Radiation Measurements, v. 41, p.
384 9-16.
385 Lai, Z.P., and Wintle, A.G., 2006, Locating the boundary between the Pleistocene and
386 Holocene in Chinese loess using luminescence: The Holocene, v. 16, p. 893-899.

Lu, H.Y., An, Z.S., Vandenberghe J., and Nugteren G., 1999, Evidence for paleoclimatic significance of grain size composite of loess deposit in central Chinese Loess Plateau, *in* An, Z., and Zhou, Z.P., eds. Proceedings of 30th International Geological Congress: VSP, The Netherlands, p. 5-10.

Maher, B.A., and Thompson R., 1991, Mineral magnetic record of the Chinese loess and paleosols: Geology, v. 19, p. 3-6.

Mejdahl, V., 1979, Thermoluminescence dating: beta-dose attenuation in quartz grains: Archaeometry, v. 21, p. 61-72.

Murray, A.S., and Olley J.M., 2002, Precision and accuracy in the optically stimulated luminescence dating of sedimentary quartz: A status review: Geochronometria, v. 21, p. 1-16.

Murray, A.S., and Wintle A.G., 2000, Luminescence dating of quartz using an improved single-aliquot regenerative-dose procedure: Radiation Measurements, v. 32, p. 57-73.

Nugteren, G., and Vandenberghe, J., 2004, Spatial climatic variability on the Central Loess Plateau (China) as recorded by grain size for the last 250 kyr: Global and Planetary Change, v. 41, p. 185-206.

Prescott, J.R., and Hutton J.T., 1994, Cosmic ray contributions to dose rates for luminescence and ESR dating: large depths and long term variations: Radiation Measurements, v. 23, p. 497-500.

Rees- Jones, J., 1995, Optical dating of young sediments using fine-grain quartz: Ancient TL, v. 13, p. 9-13.

Roberts, H.M., and Duller G.A.T., 2004, Standardised growth curves for optical dating of sediment using multiple-grain aliquots: Radiation Measurements, v. 38, p. 241-252.

410 Roberts, H.M., and Wintle, A.G., 2001, Equivalent dose determinations for polymineralic
411 fine-grains using the SAR protocol: application to a Holocene sequence of the Chinese
412 Loess Plateau: Quaternary Science Reviews, v. 20, 859-863.
413 Stevens, T., Armitage, S.J., Lu, H., and Thomas D.S.G., 2006, Sedimentation and
414 diagenesis of Chinese loess: Implications for the preservation of continuous high-resolution
415 climate records: Geology, v. 34, p. 849-852.
416 Stevens, T., Armitage, S.J., Lu, H., and Thomas D.S.G., 2007a, Examining the potential of
417 high sampling resolution OSL dating of Chinese loess: Quaternary Geochronology, 2, 15-
418 22.
419 Stevens, T., Thomas, D.S.G., Armitage, S.J., Lunn, H.R., and Lu H., 2007b, Reinterpreting
420 climate proxy records from late Quaternary Chinese loess: A detailed OSL investigation.
421 Earth-Science Reviews, v. 80, p. 111-136.
422 Stokes, S., Hetzel, R., Bailey, R.M., Tao, M.X., 2003, Combined IRSL-OSL single aliquot
423 regeneration (SAR) equivalent dose (D_e) estimates from source proximal Chinese loess:
424 Quaternary Science Reviews, v. 22, p. 975-983.
425 Sun, D., 2004, Monsoon and westerly circulation changes recorded in the late Cenozoic
426 aeolian sequences of Northern China: Global and Planetary Change, v. 41, p. 63-80.
427 Sun D., Bloemendal, J., Rea, D.K., Vandenberghe, J., Jiang, F., An, Z., and Su R., 2002,
428 Grain-size distribution function of polymodal sediments in hydraulic and aeolian
429 environments, and numerical partitioning of the sedimentary components. Sedimentary
430 Geology, v. 152, p. 263-277.
431 Sun, J., 2002, Provenance of loess material and formation of loess deposits on the Chinese
432 Loess Plateau: Earth and Planetary Science Letters, v. 203, p. 845-859.

Zhang, X.Y., Gong, S.L., Zhao, T.L., Arimoto, T., Wang, Y.Q., and Zhou Z.J., 2003, Sources of Asian dust and role of climate change versus desertification in Asian dust emission: Geophysical Research Letters, v. 30, p. 2272.

TABLES

Table DR1. Mean (L_x/T_x)*TD (in Gy) values ± 1σ for each SGC applied in this study. Also shown are regeneration points (Gy) and number of aliquots used (n)

Regen point	(L_x/T_x)*TD	±	n
Beiguoyuan 0.3-5.4 m			
5 Gy	5.42	0.06	121
10 Gy	10.2	0.10	121
20 Gy	18.7	0.15	121
50 Gy	37.9	0.22	121
100 Gy	59.6	0.32	121
Beiguoyuan 5.4-12.6 m			
10 Gy	20.5	0.133	65
20 Gy	40.4	0.20	134
50 Gy	63.4	0.31	134
100 Gy	79.5	0.40	134
150 Gy	92.0	0.70	134
Xunyi			
20 Gy	23.19	0.06	135
50 Gy	43.7	0.10	135
100 Gy	65.6	0.20	135
150 Gy	80.6	0.31	108
200 Gy	91.7	0.39	108

Table DR2. Optical dating results. Showing sample code, sampling depth, U-, Th- and K- concentrations, cosmic dose, total dose rate, equivalent dose (D_e), number of samples (n) and the age.[a] Dating results for Beiguoyuan between 30 and 330 cm are first reported in Stevens et al. (2006).

Sample	Depth (cm)	U (ppm)	Th (ppm)	K (%)	Cosmic (Gy ka^{-1})	Dose rate (Gy/ka)	D_e (Gy)	n	Age (ka)
Beiguoyuan (CH04/1/)									
CH04/1/1	30-40	2.32±0.07	10.29±0.31	1.68±0.05	0.24±0.01	3.21±0.12	25.4±1.0	13	7.9±0.4
CH04/1/2	40-50	2.31±0.07	10.16±0.31	1.70±0.05	0.23±0.01	3.22±0.12	24.3±1.0	12	7.6±0.4
CH04/1/3	50-60	2.30±0.07	10.05±0.30	1.68±0.05	0.23±0.01	3.18±0.12	31.0±1.1	14	9.8±0.5
CH04/1/4	60-70	2.34±0.08	10.61±0.32	1.70±0.05	0.23±0.01	3.25±0.12	26.5±1.5	14	8.1±0.5
CH04/1/5	70-80	2.27±0.07	10.41±0.32	1.70±0.05	0.22±0.01	3.22±0.12	31.7±1.2	14	9.9±0.5
CH04/1/6	80-90	2.26±0.10	10.37±0.36	1.65±0.05	0.22±0.01	3.16±0.12	46.1±1.7SGC	12	14.6±0.8
CH04/1/7	90-100	2.33±0.07	10.34±0.32	1.71±0.05	0.22±0.01	3.23±0.12	42.8±1.4	14	13.3±0.7
CH04/1/8	100-110	2.33±0.07	10.12±0.31	1.73±0.05	0.21±0.01	3.23±0.12	51.7±3.0SGC	11	16.0±1.1
CH04/1/9	110-120	2.35±0.07	9.84±0.30	1.69±0.05	0.21±0.01	3.17±0.12	58.7±1.6	14	18.5±0.9
CH04/1/11	130-140	2.08±0.07	9.38±0.28	1.75±0.05	0.21±0.01	3.11±0.12	58.4±2.1	13	18.8±1.0
CH04/1/12	140-150	2.20±0.07	9.60±0.29	1.76±0.05	0.20±0.01	3.17±0.12	54.4±1.8SGC	23	17.2±0.9
CH04/1/13	150-160	2.09±0.06	9.30±0.28	1.75±0.05	0.20±0.01	3.10±0.12	56.3±2.1	13	18.1±1.0
CH04/1/14	160-170	2.18±0.08	9.83±0.30	1.77±0.05	0.20±0.01	3.18±0.12	56.5±1.8SGC	10	17.7±0.9
CH04/1/15	170-180	2.13±0.07	9.45±0.29	1.70±0.05	0.20±0.01	3.08±0.12	61.1±2.0	14	19.9±1.0
CH04/1/16	180-190	2.19±0.07	9.68±0.30	1.73±0.05	0.19±0.01	3.13±0.12	58.4±1.9SGC	24	18.7±0.9
CH04/1/17	190-200	2.26±0.07	9.47±0.29	1.76±0.05	0.19±0.01	3.16±0.12	63.1±2.8	13	20.0±1.2
CH04/1/18	200-210	2.28±0.07	9.90±0.30	1.77±0.05	0.19±0.01	3.20±0.12	59.7±2.1SGC	12	18.6±1.0
CH04/1/19	210-220	2.24±0.07	9.79±0.30	1.75±0.05	0.19±0.01	3.17±0.12	62.4±1.3	13	19.7±0.9
CH04/1/20	220-230	2.26±0.07	9.84±0.30	1.78±0.05	0.18±0.01	3.20±0.12	63.4±4.3SGC	11	19.8±1.5
CH04/1/21	230-240	2.29±0.07	9.83±0.30	1.81±0.05	0.18±0.01	3.23±0.12	63.7±5.4	11	19.7±1.8
CH04/1/22	240-250	2.30±0.07	9.96±0.30	1.83±0.06	0.18±0.01	3.26±0.12	67.9±2.0	14	20.8±1.0
CH04/1/23	250-260	2.34±0.07	10.04±0.30	1.85±0.06	0.18±0.01	3.30±0.13	68.1±4.4SGC	12	20.7±1.5
CH04/1/24	260-270	2.38±0.07	10.25±0.31	1.82±0.05	0.17±0.01	3.29±0.13	66.6±2.9SGC	12	20.2±1.2
CH04/1/25	270-280	2.44±0.08	10.25±0.31	1.87±0.06	0.17±0.01	3.37±0.13	68.8±2.5	14	20.3±1.1
CH04/1/26	280-290	2.40±0.07	10.07±0.30	1.83±0.06	0.17±0.01	3.28±0.13	66.9±3.4SGC	12	20.4±1.3
CH04/1/27	290-300	2.45±0.07	10.02±0.31	1.80±0.05	0.17±0.01	3.27±0.12	66.3±4.3	13	20.3±1.5
CH04/1/28	300-310	2.28±0.07	9.57±0.29	1.82±0.05	0.16±0.01	3.20±0.12	64.5±3.0SGC	12	20.1±1.2
CH04/1/29	310-320	2.31±0.07	9.65±0.29	1.78±0.05	0.16±0.01	3.18±0.12	71.9±2.4SGC	19	22.6±1.2
CH04/1/30	320-330	2.39±0.08	10.13±0.31	1.79±0.05	0.16±0.01	3.25±0.12	64.8±1.7SGC	27	20.0±0.9

CH04/1/31	330-340	3.12±0.10	9.37±0.32	1.80±0.05	0.16±0.01	3.39±0.13	79.6±2.3SGC	19	23.5±1.1
CH04/1/32	340-350	2.79±0.08	9.43±0.31	1.79±0.05	0.16±0.01	3.30±0.13	77.6±2.9SGC	21	23.5±1.3
CH04/1/33	350-360	2.75±0.09	9.66±0.34	1.83±0.06	0.15±0.01	3.33±0.13	78.6±3.3SGC	10	23.6±1.3
CH04/1/34	360-370	2.83±0.09	10.51±0.36	1.86±0.06	0.15±0.01	3.45±0.13	75.5±4.1SGC	11	21.9±1.5
CH04/1/35	370-380	3.44±0.10	10.03±0.31	1.83±0.06	0.15±0.01	3.55±0.14	76.2±5.0SGC	10	21.5±1.6
CH04/1/36	380-390	2.75±0.11	9.79±0.30	1.73±0.05	0.15±0.01	3.25±0.13	72.0±3.4SGC	10	22.1±1.3
CH04/1/37	390-400	2.97±0.09	10.31±0.33	1.80±0.05	0.15±0.01	3.41±0.13	69.4±2.1	13	20.3±1.1
CH04/1/38	400-410	3.29±0.10	9.58±0.29	1.75±0.05	0.15±0.01	3.39±0.13	71.7±2.7	12	21.1±1.2
CH04/1/39	410-420	4.20±0.13	9.72±0.30	1.79±0.05	0.14±0.01	3.69±0.15	67.5±2.5SGC	12	18.3±1.0
CH04/1/40	420-430	3.29±0.11	9.93±0.35	1.78±0.05	0.14±0.01	3.44±0.13	75.9±4.0SGC	11	22.1±1.5
CH04/1/41	430-440	3.13±0.10	10.33±0.31	1.79±0.05	0.14±0.01	3.44±0.13	74.5±2.5	14	21.5±1.1
CH04/1/42	440-450	3.53±0.11	10.89±0.33	1.92±0.06	0.14±0.01	3.71±0.15	85.1±1.7SGC	24	23.0±1.0
CH04/1/43	450-460	3.33±0.10	9.61±0.30	1.82±0.05	0.14±0.01	3.46±0.13	73.6±3.8	13	21.3±1.4
CH04/1/44	460-470	2.95±0.10	9.40±0.29	1.88±0.06	0.13±0.01	3.39±0.13	69.3±4.2SGC	11	20.4±1.5
CH04/1/45	470-480	4.54±0.14	9.85±0.30	1.79±0.05	0.13±0.01	3.78±0.15	71.6±3.3SGC	11	19.0±1.5
CH04/1/46	480-490	6.73±0.20	10.26±0.31	1.73±0.05	0.13±0.01	4.33±0.20	78.9±2.4SGC	12	18.2±1.0
CH04/1/47	490-500	3.41±0.11	9.95±0.30	1.69±0.05	0.13±0.01	3.39±0.13	78.4±2.6	12	22.1±1.2
CH04/1/48	500-510	3.79±0.11	11.08±0.35	1.99±0.06	0.13±0.01	3.85±0.15	71.2±2.0SGC	12	18.5±0.9
CH04/1/49	510-520	3.78±0.12	10.08±0.31	1.74±0.05	0.13±0.01	3.54±0.14	70.0±2.1	12	19.8±1.0
CH04/1/50	520-530	3.33±0.11	10.47±0.33	1.81±0.05	0.13±0.01	3.51±0.14	76.0±2.6	7	21.7±1.1
CH04/1/50i	530	2.79±0.10	9.81±0.30	1.81±0.05	0.12±0.01	3.31±0.13	76.0±2.1	16	23.0±1.1
CH04/1/52	550	2.69±0.08	10.21±0.33	1.82±0.05	0.12±0.01	3.32±0.13	61.9±1.6SGC	12	18.7±0.9
CH04/1/54	570	2.61±0.08	9.97±0.31	1.92±0.06	0.12±0.01	3.37±0.13	65.5±2.6	15	19.5±1.1
CH04/1/56	610	2.71±0.08	10.16±0.31	1.85±0.06	0.11±0.01	3.34±0.13	66.1±3.6SGC	12	19.8±1.3
CH04/1/58	650	3.14±0.10	10.05±0.30	1.85±0.06	0.11±0.01	3.45±0.13	72.1±1.9	14	20.9±1.0
CH04/1/60	690	2.91±0.09	10.14±0.32	1.93±0.06	0.10±0.01	3.45±0.13	74.9±1.9	13	21.7±1.0
CH04/1/62	730	2.97±0.10	10.27±0.33	1.83±0.06	0.10±0.01	3.38±0.13	79.9±2.9SGC	11	23.6±1.3
CH04/1/64	770	2.94±0.09	10.45±0.32	1.93±0.06	0.09±0.00	3.49±0.14	81.0±2.1SGC	12	23.3±1.1
CH04/1/66	810	3.32±0.10	10.17±0.31	1.88±0.06	0.09±0.00	3.51±0.14	81.8±3.8	13	23.3±1.4
CH04/1/68	850	3.08±0.09	10.58±0.33	1.93±0.06	0.09±0.00	3.52±0.14	87.7±2.2	12	24.9±1.2
CH04/1/70	880	3.40±0.10	11.37±0.34	2.17±0.07	0.08±0.00	3.89±0.15	98.4±2.0	13	25.3±1.1
CH04/1/72	900	3.00±0.09	10.38±0.32	2.03±0.06	0.08±0.00	3.57±0.14	92.9±2.7SGC	12	26.0±1.3
CH04/1/74	920	3.12±0.09	10.94±0.34	2.03±0.06	0.08±0.00	3.64±0.14	104.3±3.0	14	28.7±1.4
CH04/1/76	940	3.17±0.10	10.79±0.33	1.96±0.06	0.08±0.00	3.58±0.14	108.1±3.7	12	30.2±1.6
CH04/1/78	960	3.49±0.11	10.81±0.33	1.91±0.06	0.08±0.00	3.62±0.14	103.4±3.5SGC	11	28.5±1.5
CH04/1/80	980	3.22±0.10	10.66±0.33	1.96±0.06	0.08±0.00	3.58±0.14	102.7±5.4SGC	12	28.7±1.9

CH04/1/82	1000	3.24±0.10	10.66±0.34	1.92±0.06	0.07±0.00	3.55±0.14	104.6±4.4SGC	12	29.5±1.7
CH04/1/84	1020	2.94±0.09	10.63±0.32	1.96±0.06	0.07±0.00	3.50±0.14	100.5±3.6SGC	12	28.7±1.5
CH04/1/86	1040	3.97±0.13	10.60±0.33	1.99±0.06	0.07±0.00	3.80±0.15	102.3±2.6SGC	13	26.9±1.3
CH04/1/88	1060	3.14±0.10	10.51±0.32	2.02±0.06	0.07±0.00	3.60±0.14	103.4±3.1	13	28.8±1.4
CH04/1/90	1080	3.18±0.10	10.43±0.32	1.97±0.06	0.07±0.00	3.55±0.14	109.4±5.1SGC	12	30.8±1.9
CH04/1/92	1100	3.86±0.12	10.48±0.32	1.93±0.06	0.07±0.00	3.71±0.15	109.7±4.0SGC	12	29.6±1.6
CH04/1/94	1120	3.91±0.12	10.39±0.32	1.90±0.06	0.07±0.00	3.68±0.15	116.7±2.6	13	31.7±1.5
CH04/1/96	1140	3.16±0.10	10.36±0.31	1.94±0.06	0.06±0.00	3.52±0.14	116.3±7.6SGC	12	33.1±2.5
CH04/1/98	1160	2.98±0.09	10.25±0.31	1.92±0.06	0.06±0.00	3.43±0.14	127.0±3.1	14	37.0±1.7
CH04/1/100	1180	3.16±0.10	10.47±0.32	1.94±0.06	0.06±0.00	3.52±0.14	121.5±2.6	13	34.5±1.6
CH04/1/102	1200	3.04±0.09	10.45±0.32	1.93±0.06	0.06±0.00	3.48±0.14	127.3±4.2	14	36.6±1.9
CH04/1/104	1220	2.84±0.09	10.14±0.32	1.87±0.06	0.06±0.00	3.34±0.13	128.8±3.4	25	38.6±1.8
CH04/1/106	1240	3.04±0.09	10.87±0.33	1.93±0.06	0.06±0.00	3.50±0.14	129.0±2.8	14	36.8±1.7
CH04/1/108	1260	2.97±0.10	10.40±0.31	1.96±0.06	0.06±0.00	3.48±0.14	138.5±3.8	14	39.8±1.9
Xunyi (CH04/3/)									
CH04/3/1	85-95	2.03±0.07	13.08±0.39	2.17±0.07	0.21±0.01	3.77±0.15	14.0±0.2	14	3.7±0.2
CH04/3/2	105-115	3.81±0.12	12.82±0.39	2.08±0.06	0.20±0.01	4.15±0.16	18.0±0.2SGC	12	4.4±0.2
CH04/3/3	125-135	2.64±0.11	12.45±0.31	2.01±0.06	0.20±0.01	3.73±0.14	29.4±0.8	14	7.9±0.4
CH04/3/4	145-155	2.99±0.11	12.22±0.37	2.13±0.06	0.19±0.01	3.91±0.15	30.6±0.3	14	7.8±0.3
CH04/3/5	165-175	3.69±0.12	10.17±0.32	1.79±0.05	0.19±0.01	3.62±0.14	49.4±1.8	12	13.6±0.7
CH04/3/6	185-195	3.89±0.12	10.87±0.36	1.84±0.06	0.18±0.01	3.77±0.15	30.4±1.1	14	8.0±0.4
CH04/3/7	205-215	3.19±0.11	9.99±0.33	1.73±0.05	0.18±0.01	3.41±0.13	57.5±2.1SGC	12	16.9±0.9
CH04/3/8	225-235	3.83±0.12	10.01±0.30	1.72±0.05	0.17±0.01	3.57±0.14	57.3±2.6SGC	12	16.0±1.0
CH04/3/9	245-255	6.71±0.20	11.37±0.35	2.18±0.07	0.17±0.01	4.87±0.21	51.2±2.0	13	14.4±0.6
CH04/3/10	265-275	2.77±0.08	10.44±0.34	2.06±0.06	0.16±0.01	3.62±0.14	82.0±2.5	14	22.6±1.1
CH04/3/11	285-295	2.62±0.08	11.04±0.35	2.13±0.06	0.16±0.01	3.68±0.14	80.7±2.5	12	21.9±1.1
CH04/3/12	305-315	2.59±0.08	11.09±0.34	1.99±0.06	0.15±0.01	3.55±0.14	83.7±2.9SGC	12	23.5±1.2
CH04/3/13	325-335	2.75±0.09	11.55±0.38	2.21±0.07	0.15±0.01	3.83±0.15	90.3±2.4SGC	24	23.6±1.1
CH04/3/14	345-355	3.41±0.10	12.07±0.36	2.20±0.07	0.15±0.01	4.03±0.16	96.6±4.5	12	23.9±1.5
CH04/3/15	365-375	2.16±0.07	7.85±0.30	1.67±0.05	0.14±0.01	2.87±0.11	99.7±6.2SGC	2	24.7±2.5
CH04/3/16	385-395	2.81±0.09	11.72±0.32	2.32±0.07	0.14±0.01	3.95±0.15	102.3±2.6	14	25.9±1.2
CH04/3/17	405-415	3.12±0.10	10.91±0.35	2.22±0.07	0.14±0.01	3.88±0.15	116.6±2.1SGC	12	30.0±1.3
CH04/3/18	425-435	2.77±0.09	10.68±0.35	2.17±0.07	0.13±0.01	3.71±0.14	125.2±3.1	14	33.7±1.5
CH04/3/19	445-455	2.73±0.09	10.79±0.33	1.96±0.06	0.13±0.01	3.51±0.14	123.2±5.9	12	35.1±2.2
CH04/3/20	465-475	2.52±0.08	11.00±0.37	2.05±0.06	0.13±0.01	3.55±0.14	134.1±1.9	14	37.7±1.6

CH04/3/21	485-495	3.06±0.09	11.24±0.34	1.98±0.06	0.12±0.01	3.65±0.14	130.1±2.1SGC	24	35.6±1.5
CH04/3/22	505-515	2.53±0.08	9.13±0.29	1.67±0.05	0.12±0.01	3.05±0.12	135.9±1.7	14	37.2±1.8
CH04/3/23	525-535	3.54±0.12	10.59±0.32	2.10±0.06	0.12±0.01	3.83±0.15	146.8±9.0	20	38.3±2.8
CH04/3/24	545-555	3.22±0.10	9.95±0.31	1.83±0.06	0.11±0.01	3.44±0.13	142.3±4.3SGC	23	41.3±2.0
CH04/3/25	565-575	2.82±0.09	10.90±0.41	2.05±0.06	0.11±0.01	3.61±0.14	147.8±2.5	14	40.9±1.7
CH04/3/26	585-595	2.86±0.09	10.59±0.32	1.97±0.06	0.11±0.01	3.52±0.14	155.0±2.0	26	44.0±1.8
CH04/3/27	605-615	2.45±0.09	11.18±0.36	2.01±0.06	0.11±0.01	3.49±0.14	158.7±7.0	12	45.3±2.7
CH04/3/28	625-635	2.94±0.09	11.08±0.34	2.03±0.06	0.10±0.01	3.63±0.14	156.1±4.8SGC	12	43.0±2.1
CH04/3/29	645-655	2.66±0.09	11.44±0.36	2.06±0.06	0.10±0.01	3.61±0.14	160.5±3.6SGC	12	44.5±2.0
CH04/3/30	665-675	2.75±0.08	10.60±0.33	1.88±0.06	0.10±0.01	3.40±0.13	157.4±2.3	26	46.4±1.9

[a]Ages and radioisotope concentrations are quoted to one standard deviation (or 10% if dispersion data is unknown), cosmic dose with 5% error and D_e to one standard error. SGC denotes a sample where the D_e has been calculated using a standardized growth curve.

Table DR3. Results of t-tests comparing L_x/T_x values for 20, 50 and 100 Gy regeneration points on SGCs from Beiguoyuan I (0-5.4 m), Beiguoyuan II (5.4-12.6 m) and Xunyi.

Test	T-calc	T-crit	P-value
Beiguoyuan I – Beiguoyuan II: 20 Gy	-10.8	±2.0	4.7×10^{-27}
Beiguoyuan I – Beiguoyuan II: 50 Gy	-9.3	±2.0	2.1×10^{-17}
Beiguoyuan I – Beiguoyuan II: 100 Gy	-9.3	±2.0	1.3×10^{-17}
Beiguoyuan I – Xunyi: 20 Gy	-27.9	±2.0	2.2×10^{-60}
Beiguoyuan I – Xunyi: 50 Gy	-24.1	±2.0	1.2×10^{-52}
Beiguoyuan I – Xunyi: 100 Gy	-16.8	±2.0	7.2×10^{-38}
Beiguoyuan II – Xunyi: 20 Gy	-22.2	±2.0	5.9×10^{-53}
Beiguoyuan II – Xunyi: 50 Gy	-18.5	±2.0	1.5×10^{-42}
Beiguoyuan II – Xunyi: 100 Gy	-7.4	±2.0	4.1×10^{-12}

Table DR4. Water contents (as proportion of wet weight) obtained during portable γ-spectrometry analysis of samples at Beiguoyuan (CH04/1/), Xunyi (CH04/3/) and Xifeng (CH04/2/) (Stevens et al., 2006). Sample numbers are also noted along with unit type (paleosol or loess).

Sample	Site	Unit	Water content
CH04/1/6-7	Beiguoyuan	Paleosol	3.7%
CH04/1/20-21	Beiguoyuan	Loess	4.6%
CH04/1/50	Beiguoyuan	Loess	2.6%
CH04/1/118	Beiguoyuan	Loess	8.5%
CH04/1/151	Beiguoyuan	Loess	1.3%
CH04/1/205	Beiguoyuan	Loess	3.2%
CH04/1/253	Beiguoyuan	Paleosol	7.2%
CH04/2/11	Xifeng	Paleosol	12.6%
CH04/2/27	Xifeng	Loess	6.2%
CH04/2/51	Xifeng	Paleosol	9.1%
CH04/2/81	Xifeng	Loess	9.2%
CH04/2/100	Xifeng	Paleosol	12.0%
CH04/2/131	Xifeng	Loess	7.6%
CH04/3/3	Xunyi	Paleosol	9.0%
CH04/3/10	Xunyi	Loess	13.1%
CH04/3/21	Xunyi	Loess	8.6%
CH04/3/27	Xunyi	Loess	6.9%
CH04/3/38	Xunyi	Loess	4.7%
CH04/3/49	Xunyi	Paleosol	12.5%
CH04/3/65	Xunyi	Loess	10.8%

Table DR5. Sedimentation rates, errors and depths for Beiguoyuan and Xunyi. Note that cm kyr^{-1} is used as in this paper ka denotes a specific age and kyr a length of time.

Depth (cm)	Sedimentation rate (cm kyr^{-1})	±
Beiguoyuan (CH04/1/)		
30-70	10.1	6.7
80-110	4.7	2.5
110-610	112.0[a]	56.0[a]
610-730	31.5	5.0
730-880	52.0	18.9
880-920	11.0	3.5
920-1100	192.9[a]	91.5[a]
1100-1260	14.8	2.5
Xunyi (CH04/3/)		
85-125	9.1	5.3
265-385	29.9	5.5
385-445	5.8	0.8
445-525	24.9[a]	12.5[a]
525-585	9.9	3.5
585-665	34.2[a]	17.1[a]

[a] Sedimentation rates calculated using slope of age model with errors set at 50%

Table DR6. Climate proxy reproducibility from repeat measurements of selected samples from Beiguoyuan (CH04/1/) and Xunyi (CH04/2/) (Stevens et al., 2006). The mean is arithmetic, calculated using the method of moments, sorting is determined using the Folk and Ward (1957) method and c.v. denotes the coefficient of variation. Errors for χ_{fd} are calculated through taking statistics of repeated calculation of χ_{fd} from repeated measurements of χ_{lf} and χ_{hf}, not through propagating errors of averaged χ_{lf} and χ_{hf} measurements (Stevens et al., 2007b).

Magnetic Susceptibility	CH04/1/2 (n=20)			CH04/1/25 (n=20)			Total (n=40)
	Mean	Stdev	c.v. (%)	Mean	Stdev	c.v. (%)	Average c.v. (%)
χ_{hf} ($10^{-8}m^3kg^{-1}$)	470.8	0.5	0.1	348.6	0.9	0.2	0.2
χ_{lf} ($10^{-8}m^3kg^{-1}$)	451.5	2.3	0.5	343.4	1.2	0.4	0.4
χ_{fd} (%)	4.1	0.5	12.1	1.5	0.5	30.3	21.2
Grain-size	CH04/2/2 (n=20)			CH04/4/10 (n=20)			Total (n=40)
	Mean	Stdev	c.v. (%)	Mean	Stdev	c.v. (%)	Average c.v. (%)
Mean (μm)	33.0	0.1	0.4	21.7	0.7	3.4	1.9
Sorting	3.0	0.0	0.3	2.9	0.0	0.5	0.4
Median (μm)	31.1	0.2	0.7	19.0	0.8	4.2	2.5
> 63 μm (%)	11.8	0.1	1.0	1.3	0.5	38.3	19.7
< 4 μm (%)	5.7	0.1	1.9	6.6	0.2	3.0	2.4
63-16 μm (%)	59.5	0.5	0.9	55.8	0.6	1.1	1.0
16-4 μm (%)	17.7	0.6	3.2	28.7	0.7	2.5	2.9
> 31 μm (%)	49.7	0.3	0.7	27.4	1.9	7.1	3.9
< 16 μm (%)	28.7	0.5	1.7	72.6	1.9	2.7	2.2
>31:16-4 μm	2.8	0.1	3.6	1.0	0.1	9.6	6.6
63-16:16-4 μm	3.4	0.1	3.8	1.9	0.1	3.6	2.9

FIGURES

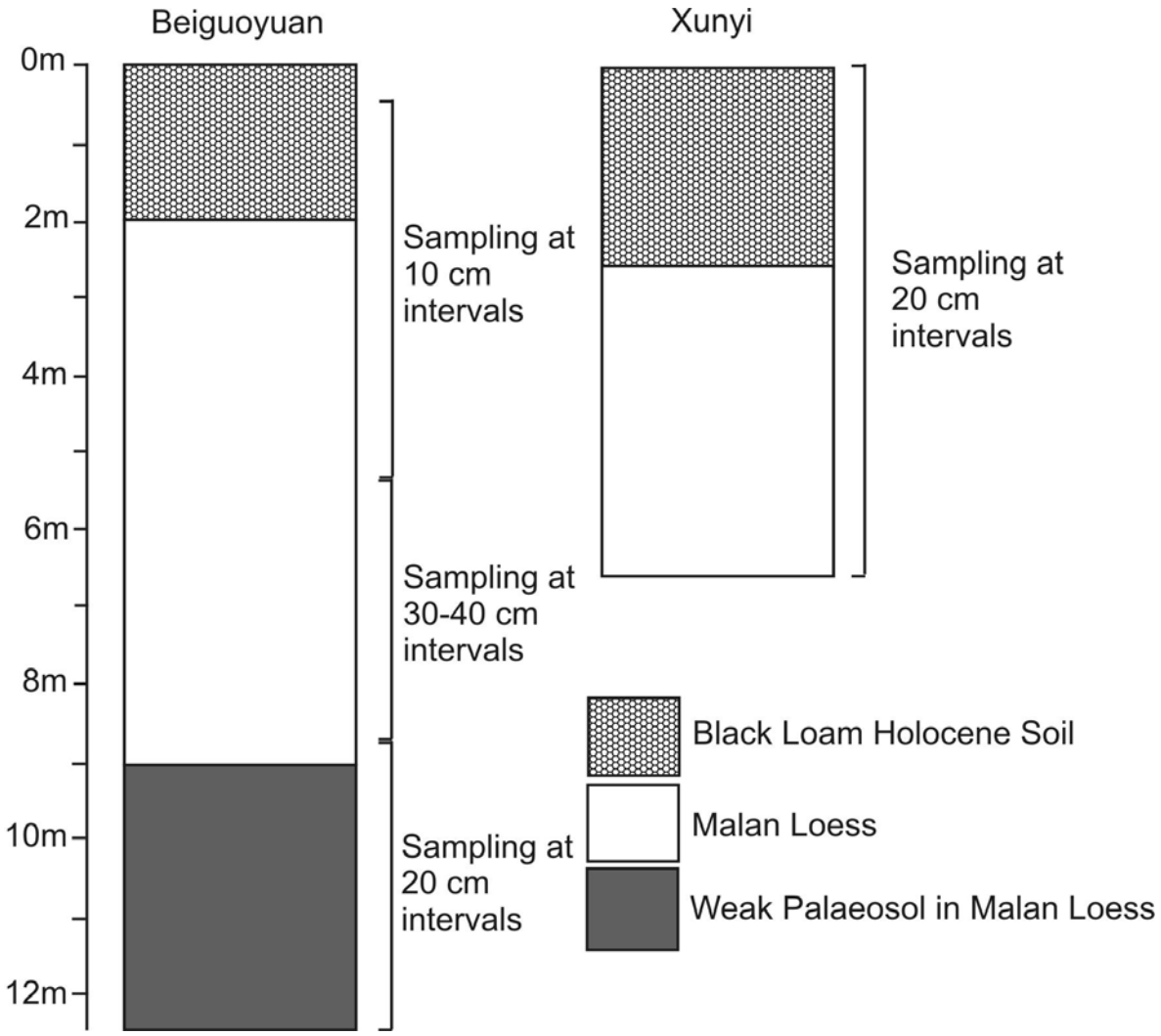

Figure DR1. Stratigraphy and sampling at study sites. The Black Loam soil is often referred to as S0 while the Malan Loess and interstratified paleosol can be correlated to L1LL1 and L1SS1 respectively.

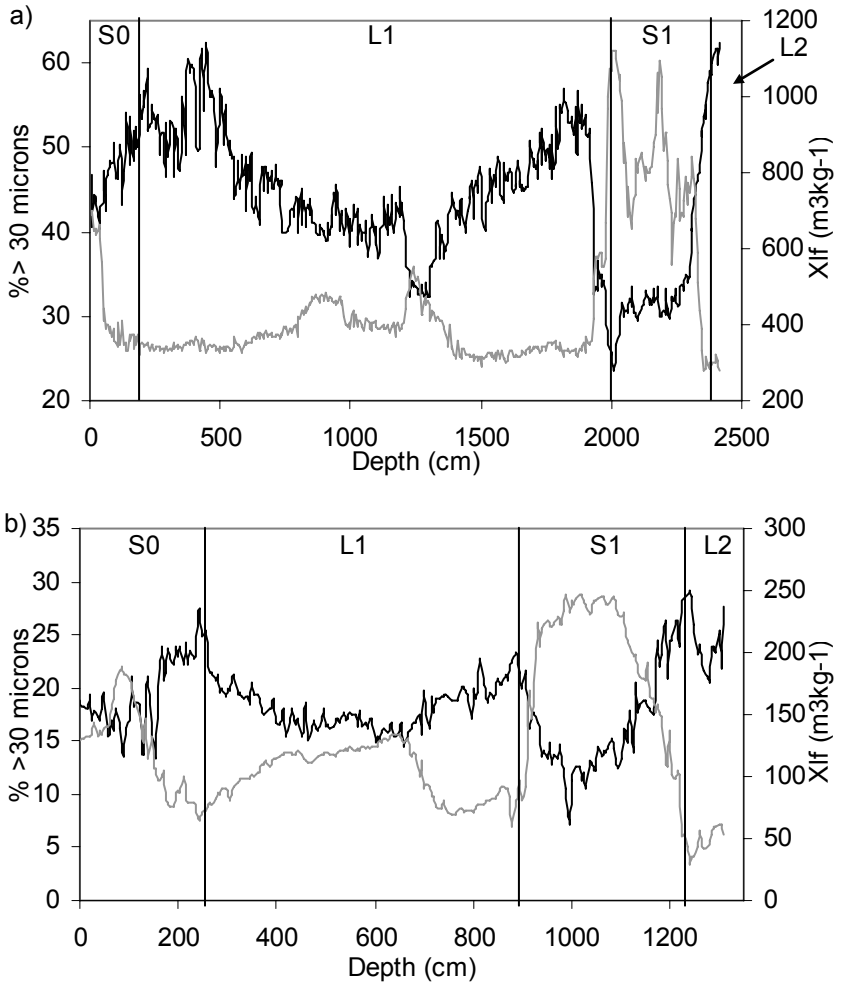

Figure DR2. Grain-size (% >30 μm – black line) and bulk low frequency magnetic susceptibility (χ_{lf} - m^3kg^{-1} – grey line) for a) Beiguoyuan and b) Xunyi plotted by depth over entire sampled strata. Stratigraphic units based on field observations are noted.

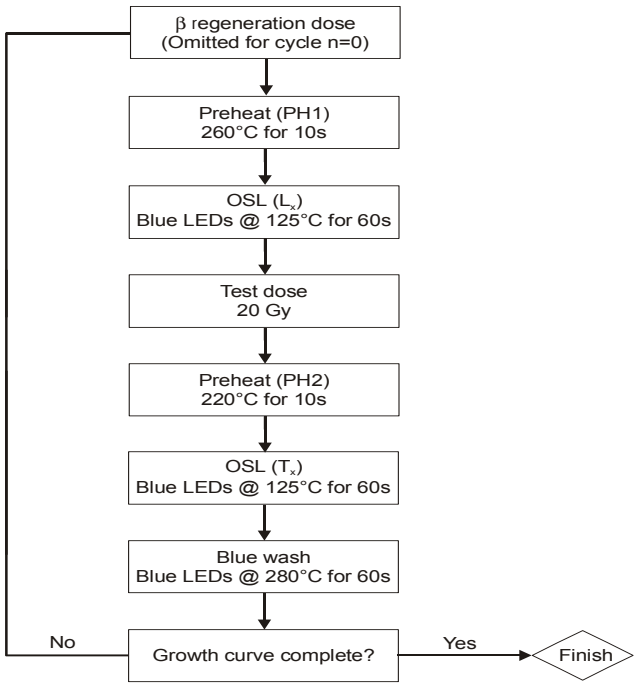

Figure DR3. Modified SAR protocol used in study. A 20 Gy test dose was used throughout.

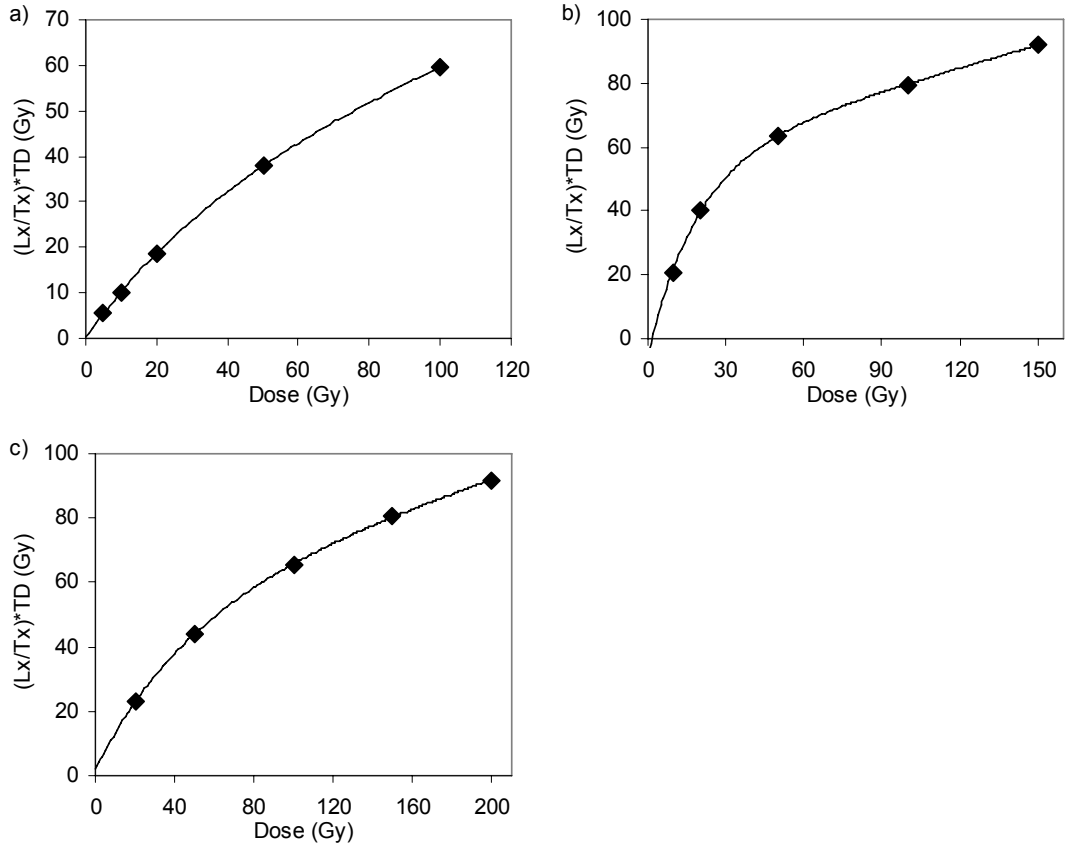

Figure DR4. Standardized Growth Curves for a) Beiguoyuan above 5.4 m, b) Beiguoyuan between 5.4 and 12.6 m and c) Xunyi. Table DR1 shows values ± 1σ for each regeneration point.

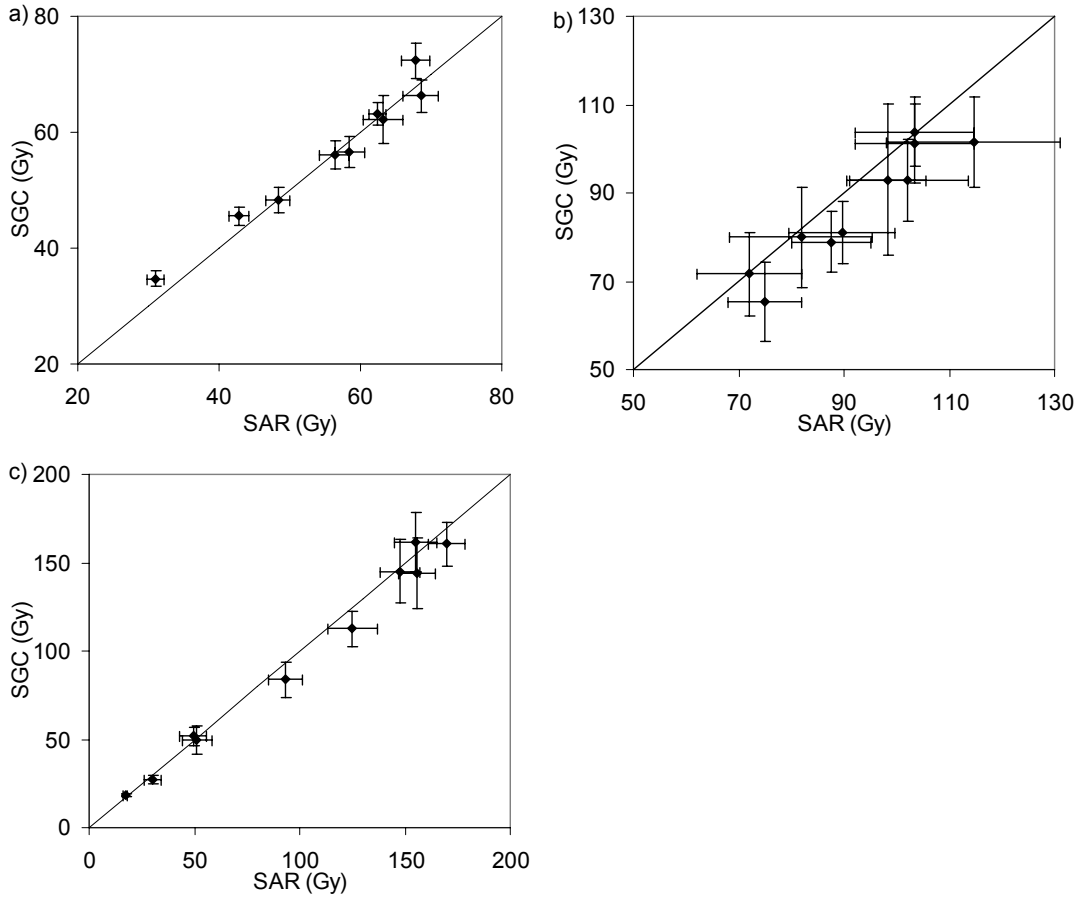

Figure DR5. Equivalent doses (Gy) of samples calculated using the relevant standardized growth curve (SGC) (Figure DR4; Table DR1) and the standard single aliquot regeneration (SAR) protocol for a) 0.3-5.4 m strata at Beiguoyuan, b) 5.4-12.6 m strata at Beiguoyuan and c) all sampled strata at Xunyi. The dark lines are 1:1 lines.

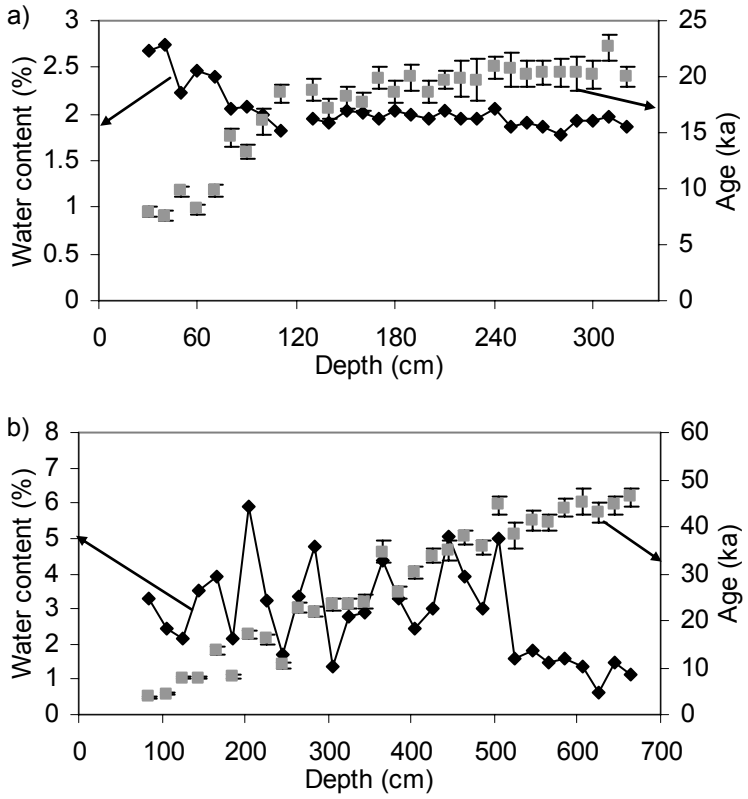

Figure DR6. Water contents (black) and OSL ages (grey) ± 1σ plotted by depth for the first 30 samples dated at the study sites (a – Beiguoyuan; b – Xunyi).

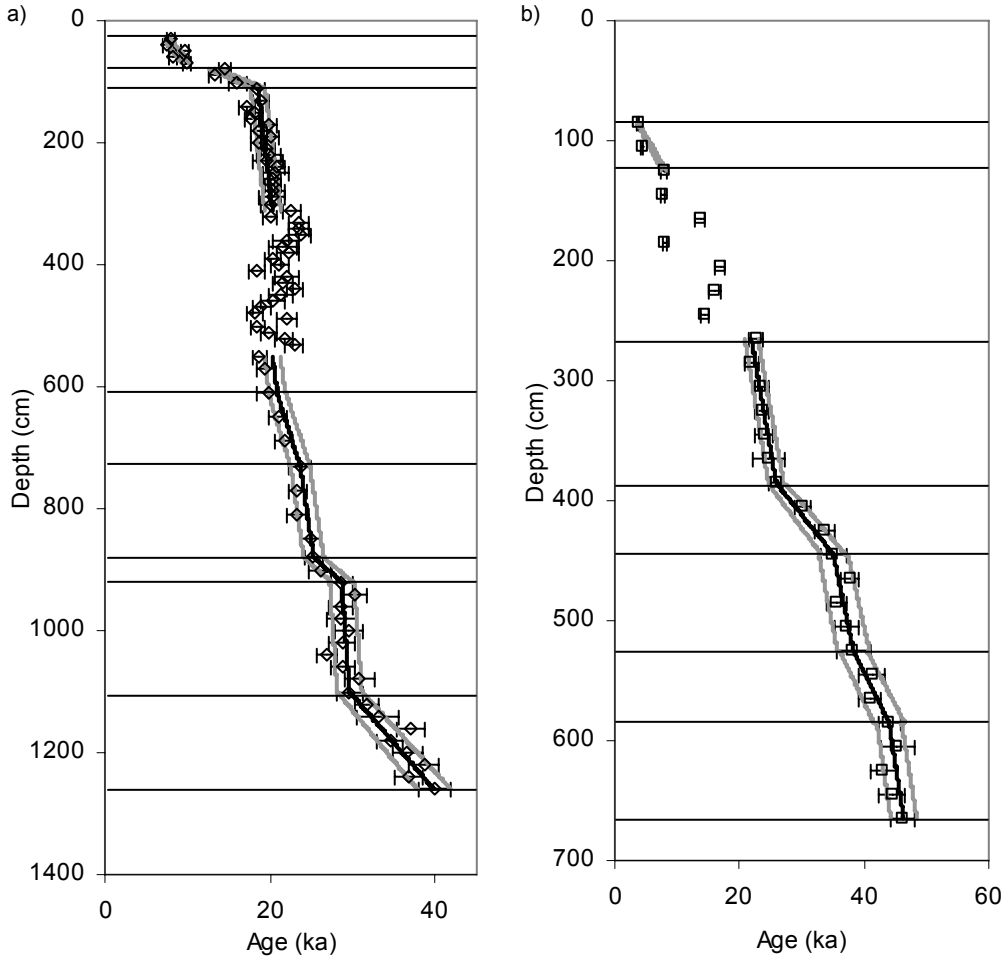

Figure DR7. OSL ages (error to 1σ) and calculated age models for a) Beiguoyuan and b) Xunyi. Error envelopes are shown in grey. Horizontal lines delineate points where changes occur in sedimentation rate. These points are used to separate strata of differing sedimentation rate in age model construction and sedimentation rate determination.

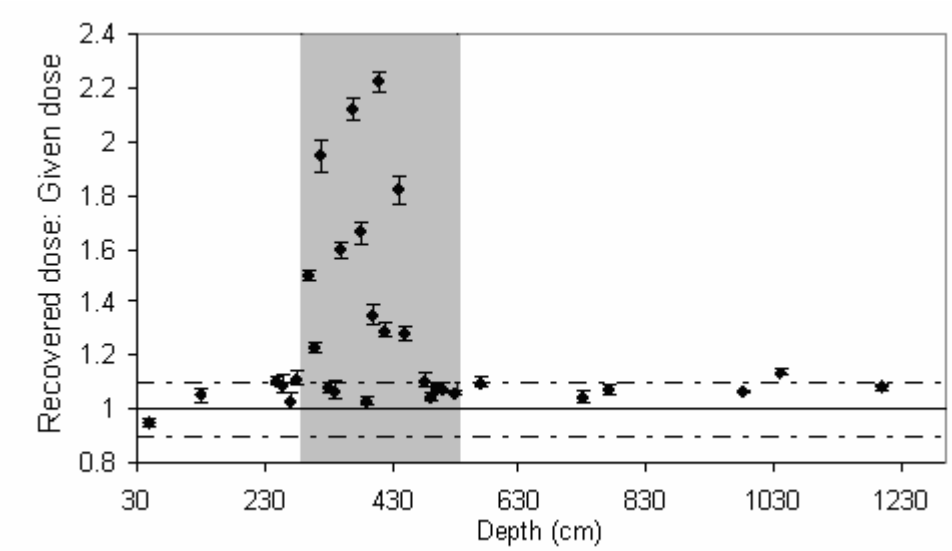

Figure DR8. Ratios of recovered to given dose for samples from Beiguoyuan plotted by depth. Shaded area denotes the location of anomalously high equivalent doses that have been excluded from age model construction. The horizontal lines indicate unity and ± 10%.

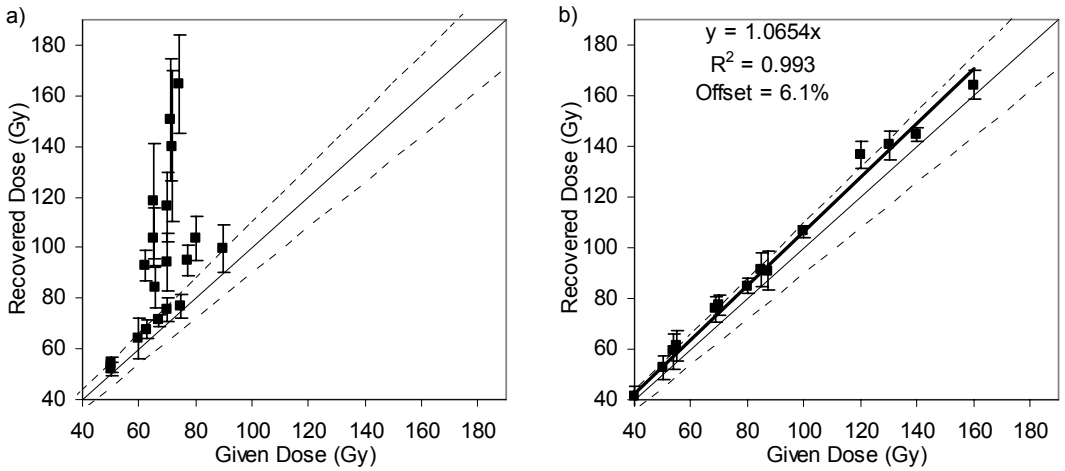

Figure DR9. Dose recovery data plotted by given and recovered dose. Samples between 3.1 and 5.2 m at Beiguoyuan are shown in a), while in b) dose recoveries for other samples in this study are shown. In b), an equation for the best fit line is shown along with the R^2 value and the % offset of the line from unity. On both parts the line of unity is shown, ±10% (dashed line).

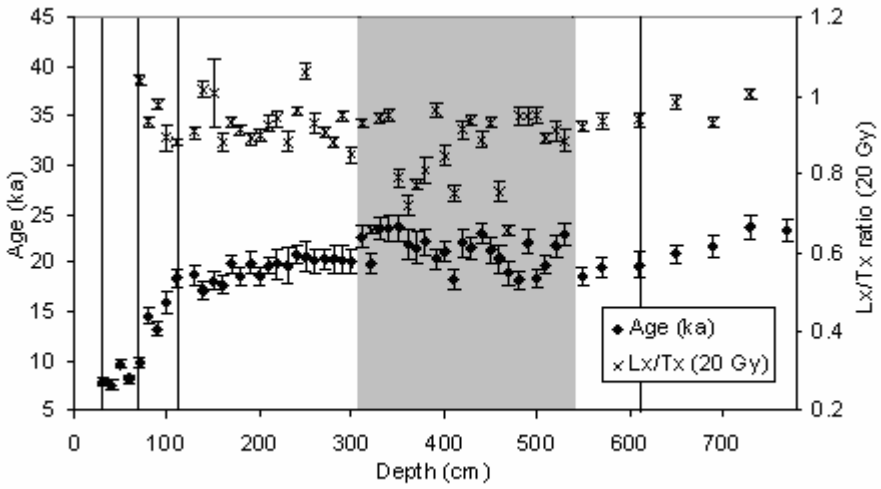

Figure DR10. Age (ka) and average L_x/T_x ratios of the first 20 Gy dose point in the SAR sequence by depth (20 Gy test dose) for Beiguoyuan. Vertical lines denote changes in sedimentation rate (see Figure DR7) and shaded area denotes area with excluded ages.

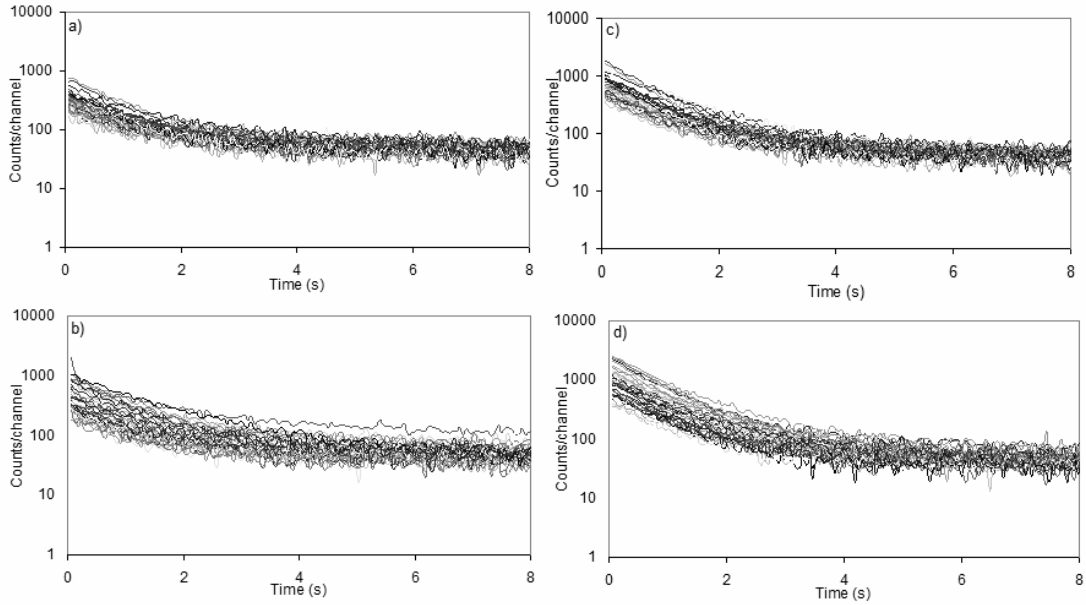

Figure DR11. 20 Gy test dose (a; b) and natural (c; d) signal decay curves plotted for multiple aliquots from samples from a) and c) surrounding strata and b) and d) age model excluded strata. OSL counts are photon counts per channel and each channel is 0.06 s. Note the log scale on the y-axis.

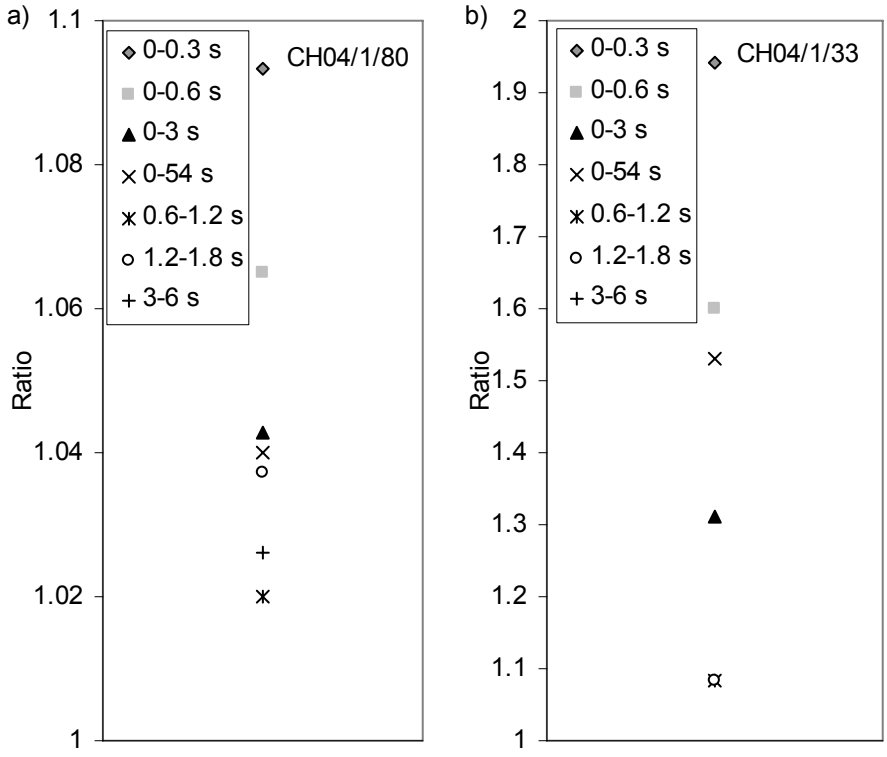

Figure DR12. Ratios of recovered to given dose for samples a) CH04/1/80 and b) CH04/1/33 from Beiguoyuan, using differing OSL signal integration limits (seconds). 0-0.6 seconds was used throughout this study.

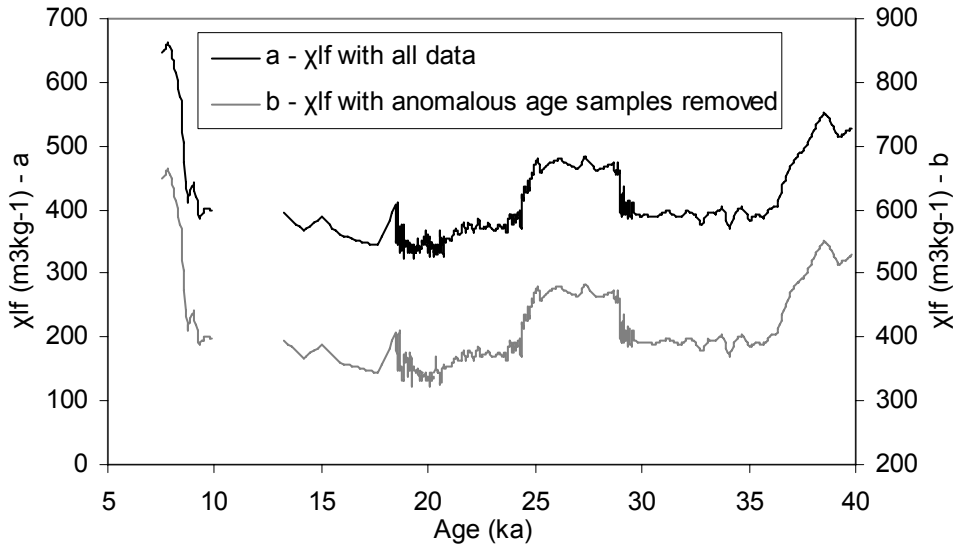

Figure DR13. Two reconstructions of the Beiguoyuan χ_{lf} data plotted by OSL age. a) shows all χ_{lf} data while b) shows χ_{lf} data without that from the excluded strata.

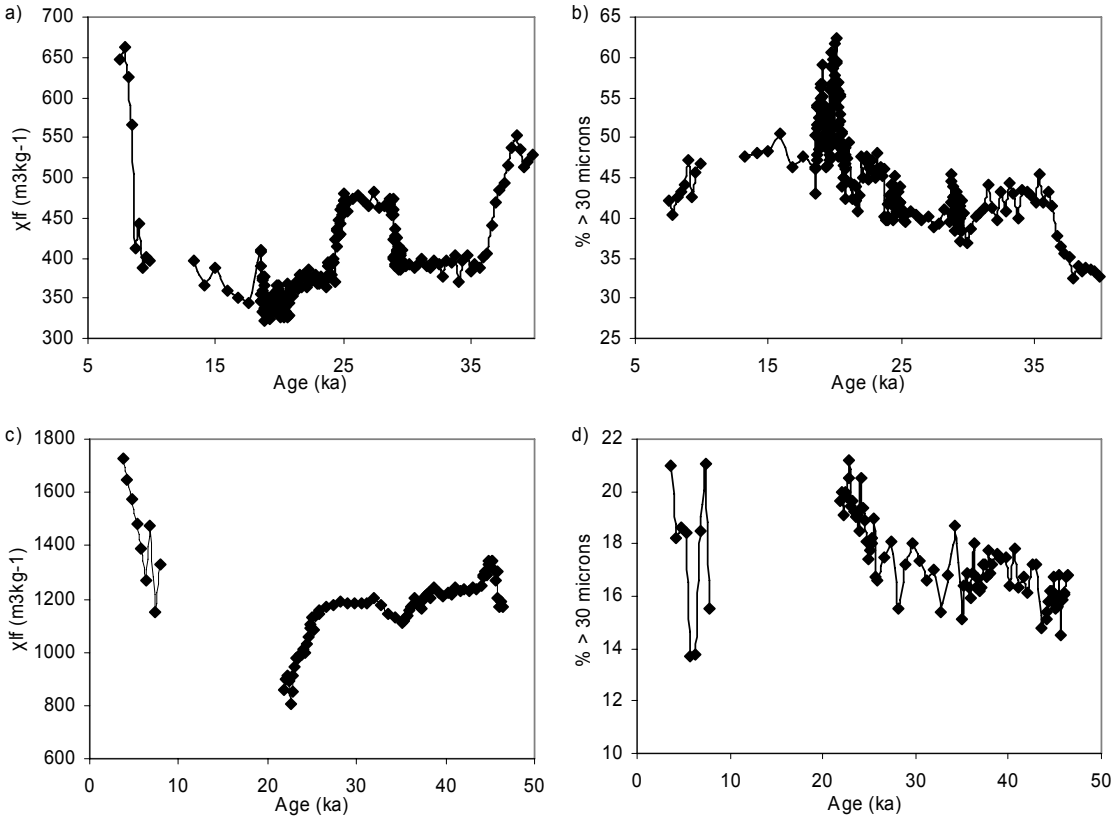

Figure DR14. a), c) Low frequency magnetic susceptibility and b), d) % of grains >30 μm plotted by OSL age for Beiguoyuan and Xunyi respectively.

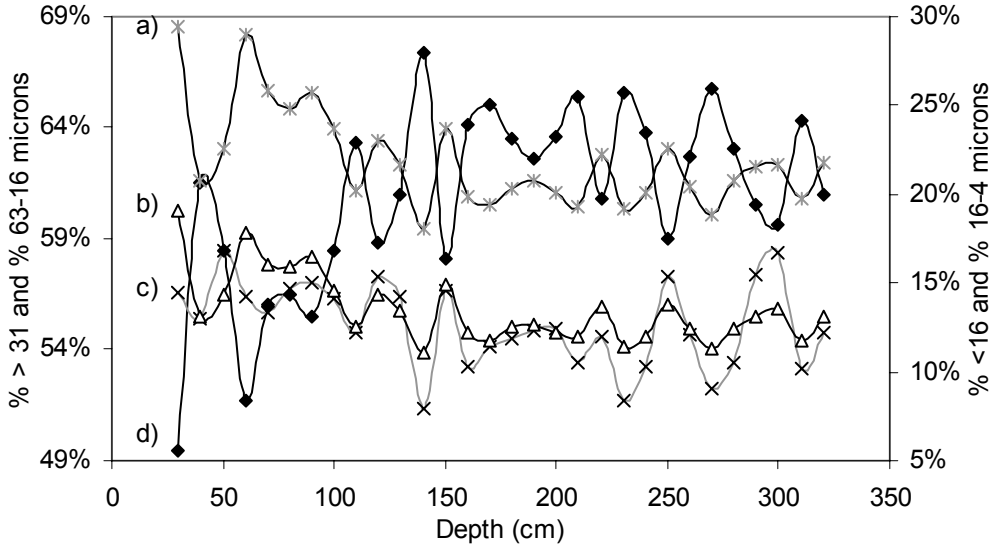

Figure DR15. Grain-size variation for upper 3.2 m of Beiguoyuan (10 cm sampling interval). Grain-size categories are a) <16 μm, b) 16-4 μm, c) 63-16 μm and d) >31 μm.